Case Studies in Construction Materials 15 (2021) e00586

Contents lists available at ScienceDirect

Case Studies in Construction Materials

journal homepage: www.elsevier.com/locate/cscm

Fire performance of innovative 3D printed concrete composite wall panels – A Numerical Study

Thadshajini Suntharalingam [a], Perampalam Gatheeshgar [a], Irindu Upasiri [b], Keerthan Poologanathan [a,*], Brabha Nagaratnam [a], Marco Corradi [a], Dilini Nuwanthika [a]

[a] Northumbria University, Newcastle upon Tyne, NE18ST, United Kingdom
[b] University of Sri Jayewardenepura, 41 Lumbini Av, Dehiwala-Mount Lavinia, Sri Lanka

ARTICLE INFO

Keywords:
3D printed concrete composite wall panels
Fire performance
Finite element modelling
Insulation fire rating

ABSTRACT

The 3-Dimensional (3D) printing technology in the construction sector has seen an accelerating growth owing to its potential advantages. For this layer-based construction, a detailed investigation on fire performance is necessary. However, there are limited research studies for 3D Printed Concrete (3DPC) walls exposed to fire. Therefore, this paper investigates the fire performance of different types of 3D printed concrete walls using validated Finite Element Models (FEMs). Validated heat transfer FEMs were extended to investigate the fire performance of a range of 3DPC wall configurations (solid, cavity, and composite) under standard fire conditions. The results show that 3DPC non-load bearing cavity walls underperform when subjected to standard fire compared to solid 3DPC walls. The novel composite 3DPC walls with the use of Rockwool as cavity insulation offers superior fire resistance.

1. Introduction

Concrete technology is one of the research areas where many novel inputs are observed. Novel types of concretes are introduced day by day depending on various applications and performance. Lightweight concrete, cellular concrete, self-consolidating concrete, self-curing concrete are few of them. Building Additive Manufacturing (BAM) which is known as 3-Dimensional Concrete Printing (3DPC) is also one of the novel types of innovative fabrication technologies of concrete which is now well established around the world [1,2]. Extrusion-based printing is a type of 3DPC which is an emerging construction technique to build the desired structure layer by layer without using any type of formwork [1,3]. The nozzles can be mounted on a gantry or a robotic arm and extrude any free form shape according to the input digital design [4–6].

This integration of digital technology into the building construction industry has exhibited remarkable transformation by changing the design and manufacturing processes (see Fig. 1). According to Peng et al. [5], 3DPC has a wealth of benefits to the construction industry in terms of increased customization with design freedom and potential productivity improvements with reduced construction time, workforce, and construction cost [1–4,6]. The ability of free form construction is the significant benefit as formwork makes up

* Corresponding author.
E-mail addresses: thadshajini.suntharalingam@northumbria.ac.uk (T. Suntharalingam), g.perampalam@northumbria.ac.uk (P. Gatheeshgar), irindu.upasiri@gmail.com (I. Upasiri), keerthan.poologanathan@northumbria.ac.uk (K. Poologanathan), brabha.nagaratnam@northumbria.ac.uk (B. Nagaratnam), marco.corradi@northumbria.ac.uk (M. Corradi), dilini.perera@northumbria.ac.uk (D. Nuwanthika).

https://doi.org/10.1016/j.cscm.2021.e00586
Received 26 February 2021;
Available online 2 June 2021

Fig. 1. World's largest 3D concrete printed building in Dubai (Apis-Cor built the office with a robotic printer, 2020 [14]).

approximately 60 % of the materials which assist in the 3DPC has been proven to save up to 60 % of construction waste, 70 % of production time and 80 % of labour costs [7]. These claims are also supported by Balletti et al. [6], who have remarked the potential need of 3DPC in combatting the demands for rapid urbanisation and the housing crisis, which is an ever growing and concerning issue.

As the research interest into 3DPC is increasing, several theories and design tools have been mainly developed to evaluate the structural performance of wall structures in 3D concrete printing processes [8–13]. However, as this technology is still in its early stages, the fire behaviour of these structures has not been investigated extensively.

Fire performance is one of the significant design aspects, which has to be explicitly evaluated to achieve the resilient and optimum design. Structural fire damage can be identified as one of the severe conditions that a structure could undergo during its life span, especially in high rise buildings. According to the literature, more than thousands of lives are lost annually due to structural fires [15, 16]. It is difficult to terminate the fire generation in structures entirely, but the damage could be minimized by limiting and delaying the fire spreading, which will give more evacuation time to occupants. When it comes to fire spreading, boundary wall material of the buildings plays a vital role. Fire and the heat transfer could be either controlled or accelerated depending on the boundary wall material.

In general, conventional concrete structures have a notable reputation for their fire performance and past researchers have studied the behaviour of concrete for fire extensively [15–19]. It is a non-combustible material, which serves as good insulation with low thermal conductivity, high heat capacity and slower strength degradation with temperature [16,19–21]. Even though well-established design guidelines and elevated temperature performance data are available for normal-weight concrete, very few literatures are found for evaluating the fire performance of 3D printed concrete.

The significance of studying the fire behaviour of 3D printed concrete structures can be discussed as follows. Though the 3DPC technology is replacing the need of conventional form poured concrete, the material behaves like a mortar rather than the typical concrete [22,23]. In addition, concrete mixes used for 3DPC have much higher strength, which is more vulnerable to spalling compared to normal concrete due to the higher binder/fine aggregate ratio and the lower water/binder ratio [11,23]. Hence, it should be tested to the same standards which align with concrete and mortar to make the results comparable. In addition, several initial researches in printable concrete show the vulnerability of the structures due to low strength at bond interfaces [24–28]. The bond strength of a 3D printed concrete specimen is interconnected with many parameters such as material viscosity, time gap between printing the layers and contact area between the successive layers [13,24,27,29]. Hence, it is important to analyse the effect of extrusion and material deposition process on the fire resistance and the behaviour of the interlayer bonding at elevated temperatures. Moreover, the fire performance of 3D printed concrete wall depends on a number of factors including the material composition, density of the material, thickness of the wall, wall configurations and the type of insulation. Wang et al. [30] evaluated the structural performance of 3D printed concrete elements with four different types of interior hollow structures. The finding of considerable mechanical strength achievement with less material from the study has driven towards the lightweight optimization of 3DP modular members for the assembly constructions. However, the behaviour of such innovative structures towards fire has to be investigated.

Fire performance of a structural element could be evaluated through three criteria—Insulation, Integrity and Structural (load bearing). An insulation criterion measures the heat transfer through the element; Integrity criteria check the fire flame penetration through the element and structural measures the load-bearing ability during the fire. Fire tests are the conventional method of determining these criteria. Element is exposed to a standard fire and unexposed surface temperature (Insulation), flame penetration (Integrity) and deflection of the element (load-bearing) are measured [16–18]. Since most of the 3D printed concrete walls are

Fig. 2. (a) Rectangular printed concrete section with 15 mm layer height; (b) 3DPC Sample; (c) Cut 3DPC Sample [31].

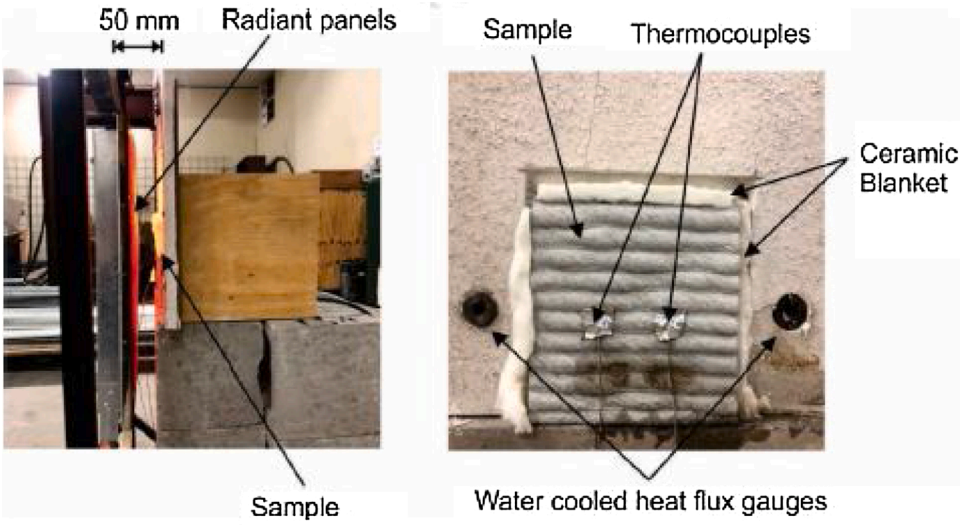

Fig. 3. Experimental setup of radiant panel setup and a 3DPC sample tested [31].

non-load bearing insulation and integrity criteria are more crucial.

In order to address the aforementioned issues, Weng et al. [31] performed an experimental study to evaluate the printability and mechanical properties of a developed 3D printable fibre reinforced cementitious material under elevated temperature. Another preliminary experimental study has been conducted by Cicione et al. [32] to investigate the behaviour of 3D printed concrete at elevated temperatures.

On the other hand, conducting fire tests are very expensive, time-consuming and destructive. Moreover, the evaluation of a structure's performance under realistic fire conditions requires advanced computational modelling [33]. Finite element method is one such method that can be utilized to determine the fire performance of structural elements. Once the developed model is validated with the experimental results, parametric variations could be done in the model and determine the fire performance variations with those parameters.

Therefore, there is an inevitable absence of standardizations and literatures to investigate the behaviour of 3D printed concrete structures at elevated temperatures. Besides, no research has been conducted to date to investigate the fire performance of 3DPC wall panels numerically. Hence, this study is focused on investigating the fire performance 3D printed concrete wall panels numerically using the experimental results presented by Cicione et al. [32].

Initially, two-dimensional and three-dimensional Heat transfer Finite Element (FE) models were developed using ABAQUS [34] finite element software. Similarly, two-dimensional heat transfer finite element model was developed using MATLAB. The developed FE models were validated against the results obtained from the available experimental study. Then the validated 3D FEM was used to

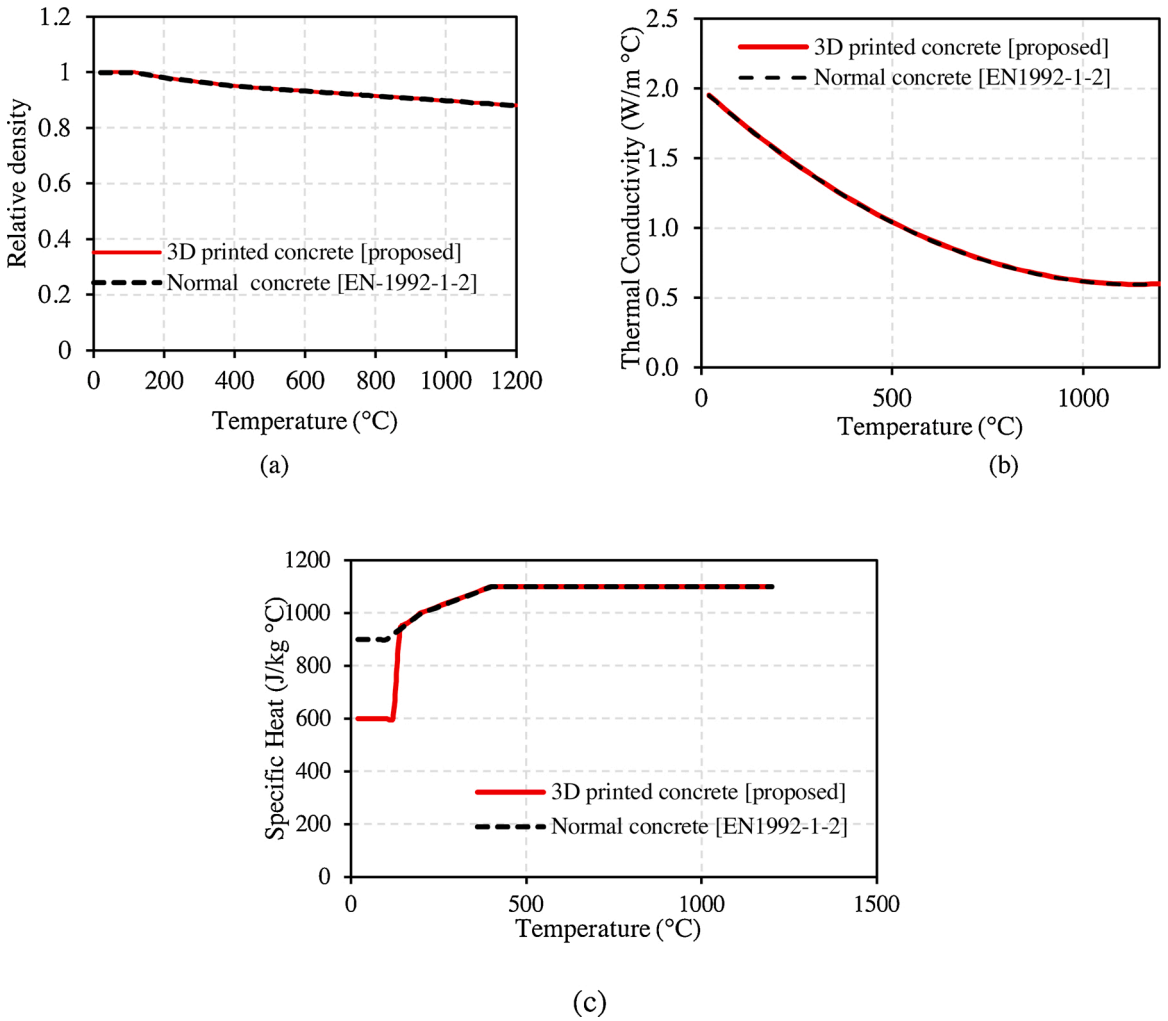

Fig. 4. Thermal properties of 3D printed concrete: (a) Relative density; (b) Thermal conductivity; (c) Specific heat.

perform a detailed parametric study to determine the insulation fire rating of non-load bearing 3D printed concrete wall panels with five different densities, four different solid wall thickness, and three different wall configurations with and without Rockwool insulation. The results of the detailed FE study of non-load bearing 3DPC walls are presented and discussed.

2. Experimental study

Cicione et al. [32] conducted a preliminary experimental investigation on the behaviour of 3D printed concrete at elevated temperatures. Both 3D printed concrete samples and mould casted concrete samples were tested. The samples were exposed to a high incident heat flux through radiant panels rather than testing them under conventional standard fire furnace conditions. This method was used to study the effect of thermal curvature and induced stresses more easily by creating thermal gradients in small samples. In addition, simplified one-dimensional heat conduction was used for the experimental setup to analyse the complex behaviour of 3D printed concrete at elevated temperatures. It was concluded that 3D printed concrete is less vulnerable to spalling as a result of higher permeability and porosity compared to conventional casted concrete. All samples cracked during the experiments and the failure was identified along the interlayers, indicating that the material strength is lower at the interface. In this study, only the results of 3D printed concrete samples were used for the numerical analysis.

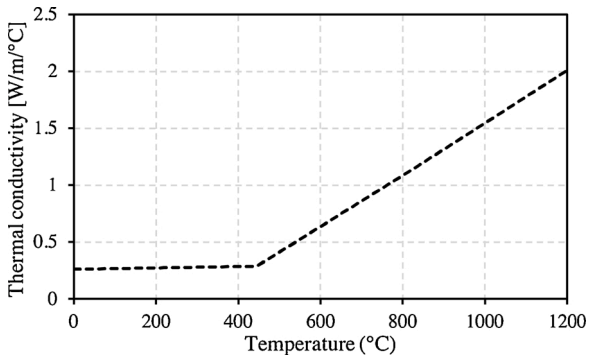

Fig. 5. Thermal conductivity of Rockwool.

2.1. Sample preparation

Experimental study has been conducted for eight samples in total including, two (2) normal concrete panels (NCC) with the dimensions of 160 × 160 × 40 mm, three (3) 3D printed concrete (3DPC) panels of 160 × 165 × 50 mm and three (3) 3D printed and cut samples to have a smooth surface (C3DPC) of 160 × 160 × 40 mm. The 160 mm wide 3D printed concrete samples were extracted from a 560 × 240 × 165 mm (Length × Width × Height) rectangular printed section as shown in Fig. 2.

2.2. Experimental setup

Direct radiation of approximately 50−60 kW/m^2 was applied through the radiant panels perpendicular to the front face of the sample (Fig. 3). Twelve (12) thermocouples had been placed on the 3D printed concrete samples; as 4 thermocouples between printed layers, 4 thermocouples within the printed layers, and 2 thermocouples on the front and back of the sample surface, respectively. The variation of temperature measurements with time on the fire exposed face (Front), middle point and unexposed face (Back) were recorded. The samples were heated until a temperature of 300 °C on the thermocouples connected to the middle of the samples. In order to ensure a 1-dimensional heat transfer, the sides of the samples were entirely covered with ceramic blanket and the backside was open to the environment. An approximate distance of 50 mm was maintained between the radiant panels and the test samples.

3. Development of finite element model

3.1. General

This section presents detail on the FE modelling of heat transfer behaviour of 3D printed concrete walls. Three types of 3D printed wall configurations: (a) solid wall; (b) cavity and (c) composite (cavity filled with insulation material) were investigated through FE analysis. The fire performance of the 3D printed concrete walls can be assessed through 1D, 2D, and 3D analysis. Simplified 1D and 2D models can be employed to simulate the fire performance assigning appropriate thermal properties and boundary conditions. However, 3D analysis is usually capable to capture the fire behaviour of full-scale walls allowing the application of partial boundary conditions, varying cavity shapes, also across the depth. This study investigates both 2D and 3D analyses of 3DPC walls exposed to fire. 2D and 3D Heat transfer FE analysis of these wall configurations were performed using a general-purpose, commercially available FE software package, ABAQUS [34]. Also, a 2D heat transfer finite element model was developed using MATLAB to determine the unexposed surface temperature variation of 3D printed concrete wall panels exposed to fire conditions.

3.2. Elevated temperature thermal properties

Thermal FE modelling development of 3D printed concrete wall configurations is hugely relying on the key controlling parameter of temperature-dependent thermal properties of the material [17,31]. Thus, the input of accurate thermal conductivity, specific heat, and relative density variations with elevated temperature govern the thermal behaviour. This study involves investigating the fire performance of 3DPC non-load bearing walls with and without cavity insulation. Therefore, the thermal properties of the 3DPC and cavity insulation are described herein.

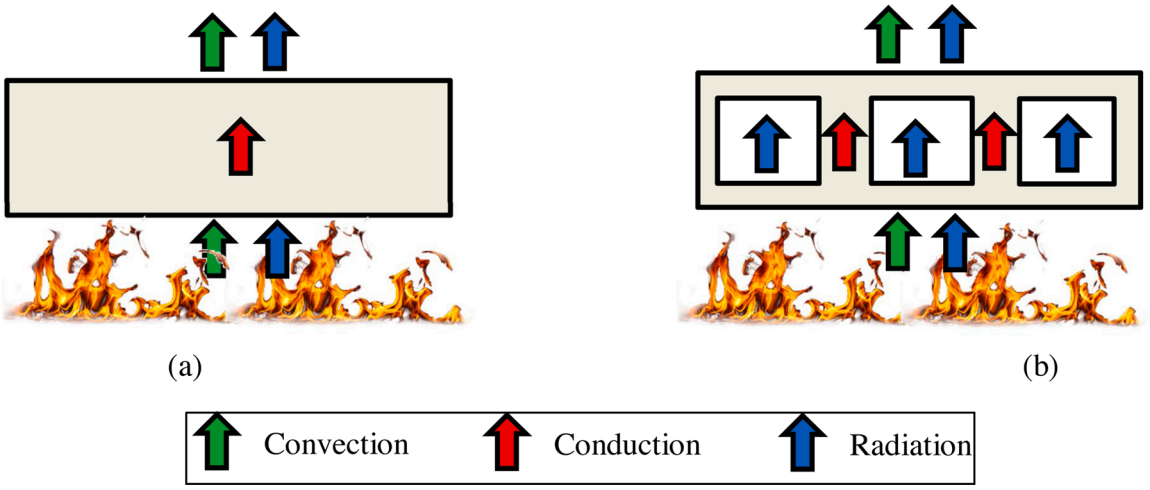

Fig. 6. Heat transfer mechanism in 3DPC walls in fire: (a) Solid wall; (b) Cavity wall.

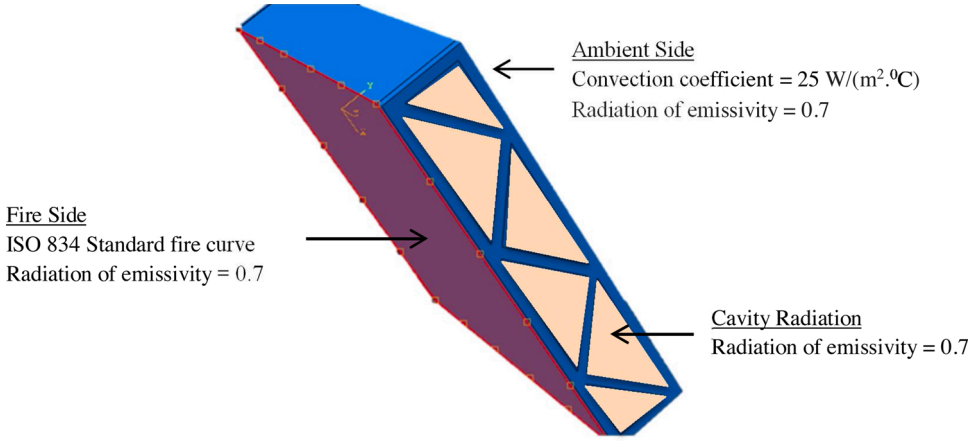

Fig. 7. Applying fire loading as a boundary condition.

EN 1992-1-2 [35] provides the thermal properties at elevated temperatures in terms of thermal conductivity, specific heat, and density of concrete with siliceous and calcareous aggregates. These temperature-dependent thermal properties were employed in the FE models with suitable modifications. It is worth to mention that specific heat variation was slightly modified within 20−120 °C temperature range while initial density (at room temperature) was considered as the density of the 3D printed concrete. These modifications were verified against the experimental fire test results of 3D printed concrete (explained in Section 4). Fig. 4 depicts the considered and proposed thermal properties of 3D printed concrete at elevated temperatures.

In construction, light steel frame walls are composed with light gauge steel studs and fire-resistant wall boards fixed on either side of the studs. Cavity enclosed by the wall boards and studs is generally filled with insulation materials such as Rockwool, glass fibre, and cellulose fibre for better fire performance in non-load bearing walls [36]. In this study, possible fire performance improvement of 3DPC

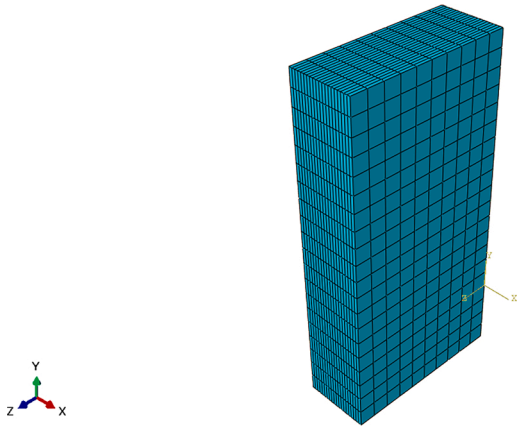

Fig. 8. Mesh refinements of Solid wall panels.

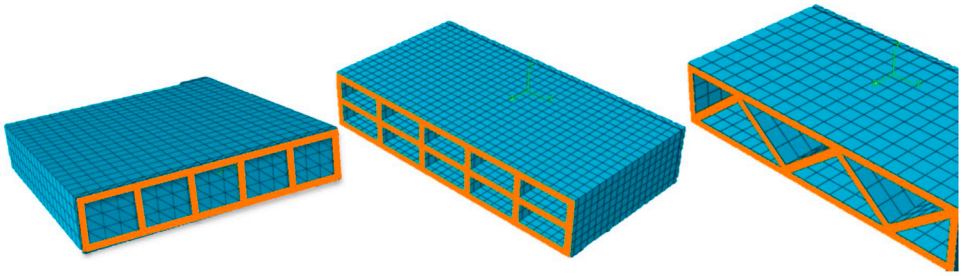

Fig. 9. Mesh refinements of Cavity wall panels.

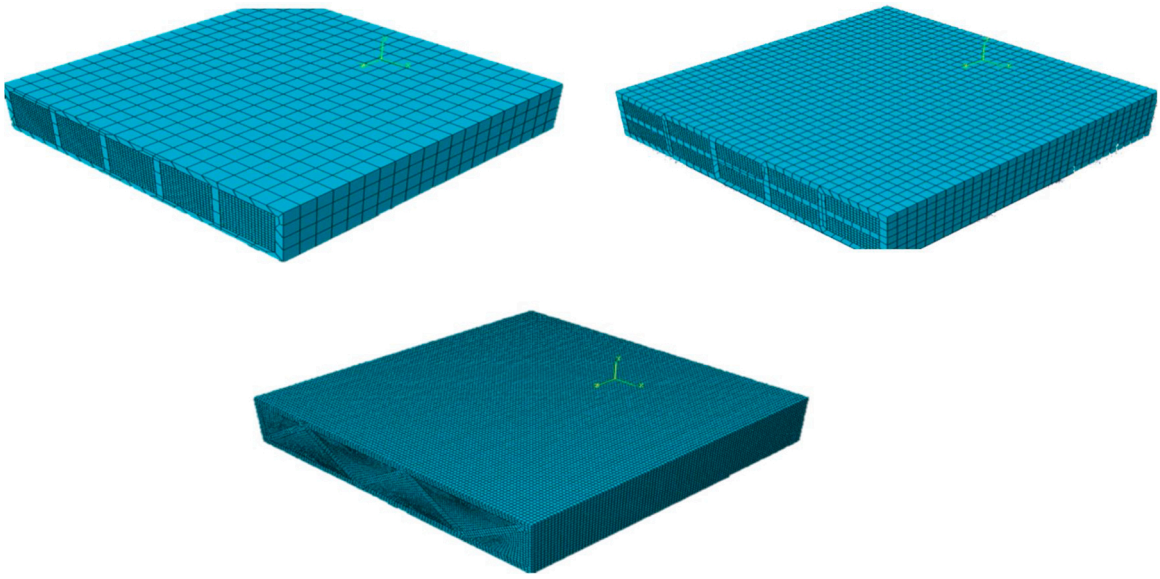

Fig. 10. Mesh refinements of cavity insulated wall panels.

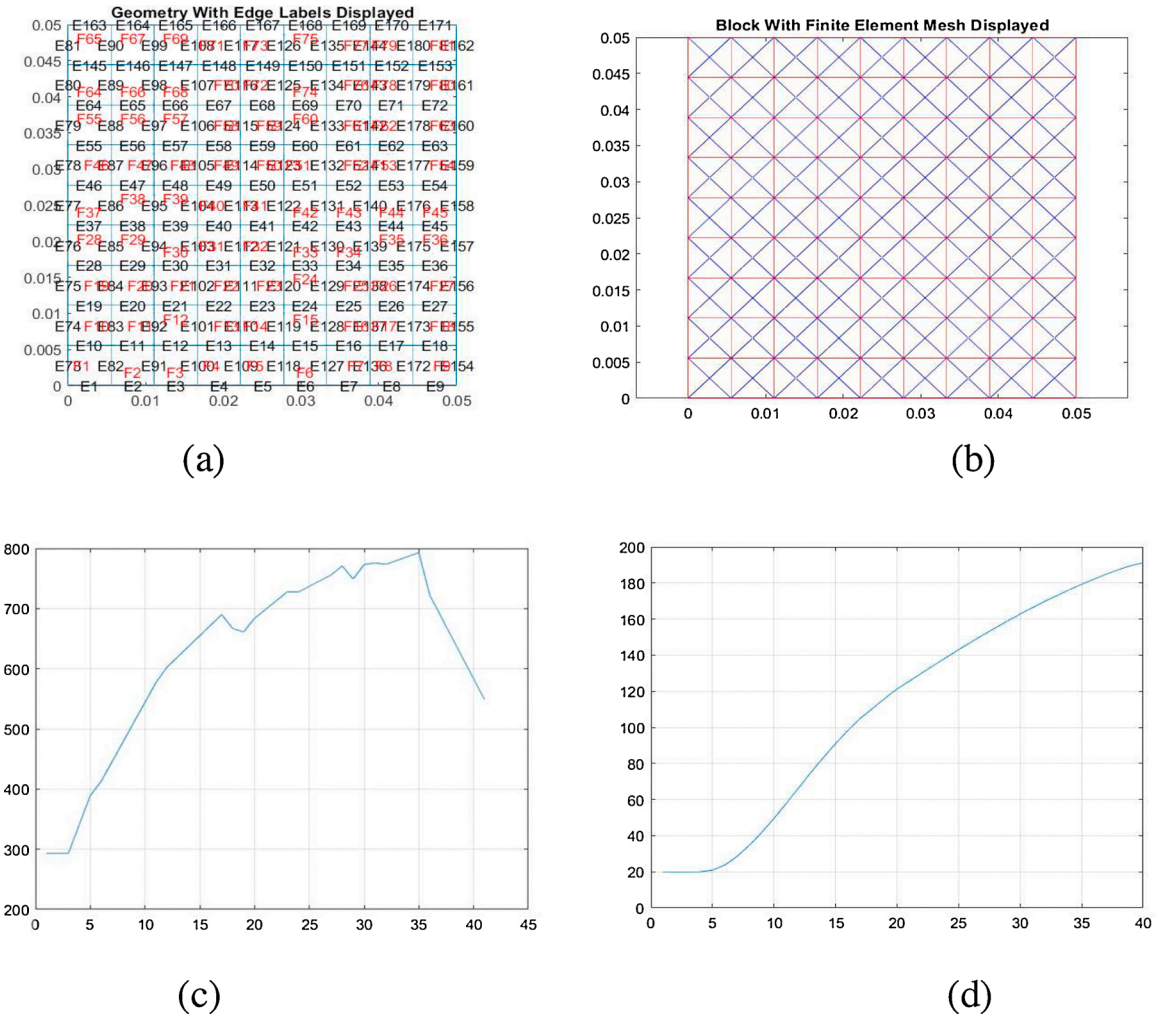

Fig. 11. Matlab modelling (a) Geometry, (b) Meshing, (c) Front side temperature variation, (d) Unexposed surface temperature (°C) variation with time (min).

cavity walls was investigated using Rockwool as insulation material. Fig. 5 illustrates the thermal conductivity variation of Rockwool insulation material. At elevated temperatures, Rockwool maintains constant density and specific heat values which are 100 kg/m^3 and 840 J/kg.°C, respectively [37].

3.3. Heat transfer model in Abaqus

3.3.1. Thermal loading and boundary conditions

Thermal loading and boundary conditions were assigned to the FE model to behave similarly to the actual conditions. This loading was applied to the 3-D printed concrete vertical wall surface as boundary condition. The time-temperature response at fire side of 3D printed concrete wall was defined to follow ISO 834 standard fire curve [38]. This was assigned using amplitude curve. Eq. (1) presents the time vs temperature response defined by the standard fire curve. Here T is the temperature at time t. The initial temperature of the 3D printed concrete wall is assumed to be room temperature.

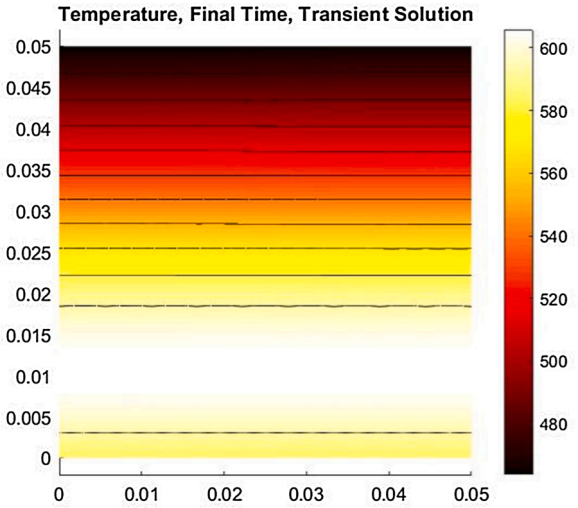

Fig. 12. Temperature contour (40 min).

$$T = 345\log_{10}(8t + 1) + 20 \tag{1}$$

Heat transfer across a 3DPC wall occurs through three major heat transfer modes, namely, conduction, convection, and radiation. All these heat transfer methods were considered in the FE models. Fig. 6 shows heat transferring methods of solid and cavity 3DPC walls. Thus, the heat flux at the boundary is calculated from temperature of the curve (T) and temperature at surface (T_a). Q_c and Q_r are heat transfer through convection and radiation hence q is the heat flux.

$$q = Q_c + Q_r \tag{2}$$

$$Q_c = h_c(T - T_a) \tag{3}$$

$$Q_r = \varepsilon\sigma\,(T^4 - T_a^4) \tag{4}$$

Where h_c is the convection coefficient of the material, ε is the relative emissivity of the material, and σ is the Stefan–Boltzmann constant (5.67×10^{-8} W/(m^2 °C^4)).

The conduction effect was incorporated into the FE models using suitable conductivity values at elevated temperatures as discussed in Section 3.2. The convection effect was simulated defining convective film coefficients. These coefficients vary for fire and ambient sides. For fire side a higher convective film coefficient value was defined while that of for ambient side is 25 W/(m^2°C) of the 3DPC walls to simulate convective heat loss to the outside environment.

The heat transfer radiation was simulated by applying a specific emissivity radiation coefficient to the 3D printed wall surfaces. For the fire and ambient side of the 3D printed wall surfaces a surface emissivity radiation of 0.7 was applied. It is noteworthy to mention that the heat transfer through the air cavity by means of conduction and convection is assumed to be negligible. When 3D printed concrete wall was subjected to fire, the air inside the enclosed cavity was motionless leading to a negligible convective heat transfer. Similarly, the low thermal conductivity of the air inside the cavity leads to negligible heat transfer by the means of conduction [39]. Thus, major source for the heat transfer within cavity is radiation enclosed by cavity surfaces. These cavity surfaces were selected and a cavity radiation emissivity of 0.7 was assigned. Similar modelling techniques were employed by past researchers [36,38,39] to model light steel frame wall configurations. The assigned boundary conditions are illustrated in Fig. 7.

3.3.2. Element type and mesh refinement

Meshing techniques and selection of suitable element type are directly related to the accuracy of the numerical model. 3D printed concrete wall and cavity insulation was modelled using heat transfer solid elements (DC3D8) which are 3D 8-node linear brick element

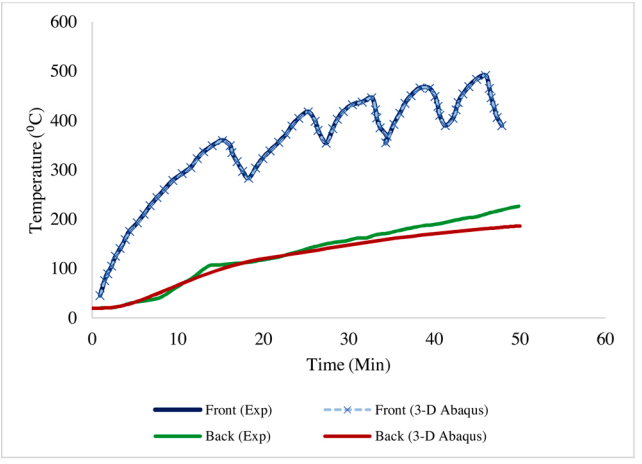

(a)

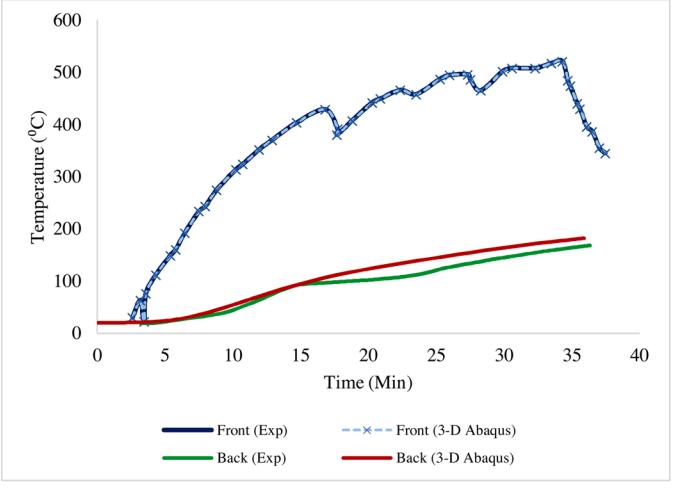

(b)

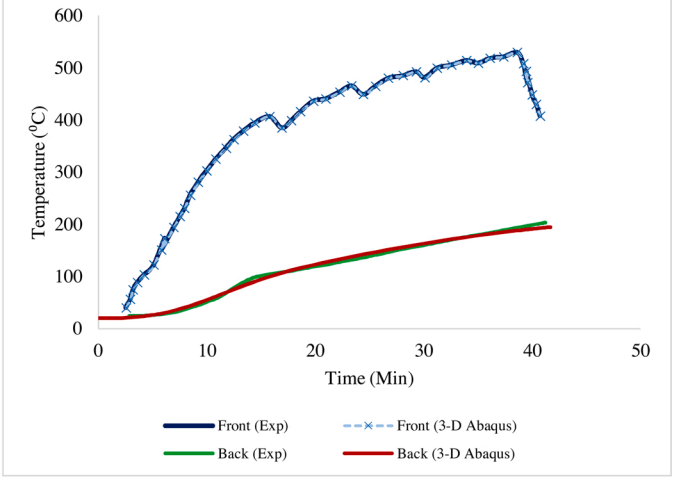

(c)

(caption on next page)

Fig. 13. (a): Comparison of Experimental results with 3-D FEA in ABAQUS results for 3DPC(S1). (b): Comparison of Experimental results with 3-D FEA in ABAQUS results for 3DPC(S2). (c): Comparison of Experimental results with 3-D FEA in ABAQUS results for 3DPC(S3).

with one degree of freedom per node. Considering the convergence of the results, mesh size was selected to capture the heat transfer across the 3DPC wall. In cavity insulated 3DPC walls continuity between the concrete and insulation material surface for heat transfer was ensured using tie constraint option available in ABAQUS. This creates a solid-solid heat transfer between them. ABAQUS FE model mesh refinements for different wall configurations such as 200 mm thickness solid wall, cavity wall panels and cavity insulated composite wall panels are shown in Figs. 8–10 respectively.

3.3.3. Solution method

To investigate the thermal behaviour, ABAQUS allows performing uncoupled and coupled thermal analysis. Coupled analysis is typically employed to investigate combined mechanical-thermal behaviour. Since, considered 3DPC wall configurations are non-load bearing, uncouple heat transfer analysis was performed. Time-temperature variations can be obtained to study the thermal response of 3DPC walls.

3.4. Heat transfer model in Matlab

MATLAB Partial Differential Equation (PDE) toolbox was used to develop the 2D heat transfer finite element model in order to determine the insulation fire rating of 3D printed concrete wall panels. Partial differential equations could be solved through finite element modelling with the aid of MATLAB PDE toolbox.

Eq. (5) is the general partial differential equation used in MATLAB PDE toolbox where m, d, c, a, f are constants and u is the variable that could be defied for a time-dependent problem.

$$m\frac{\partial^2 u}{\partial t^2} + d\frac{\partial u}{\partial t} - c\nabla^2 u + au = f \tag{5}$$

The governing partial differential equation in a heat transfer problem is given in Eq. (6) where ρ is the material density, C_p is the material-specific heat, k is the material thermal conductivity, T is the temperature, t is the time, t_z is the thickness and Q_c and Q_r are heat transfer through convection and radiation.

$$\rho C_p t_z \frac{\partial T}{\partial t} - kt_z\nabla^2 T + 2Q_c + 2Q_r = 0 \tag{6}$$

Q_c and Q_r in the Eq. (6) are defined in the Eqs. (3) and (4). Hence, the complete heat transfer governing equation can be derived as in Eq. (7).

$$\rho C_p t_z \frac{\partial T}{\partial t} - kt_z\nabla^2 T + 2h_c T + 2\varepsilon\sigma T^4 = 2h_c T_a + 2\varepsilon\sigma T_a^4 \tag{7}$$

Hence, the modified partial differential equation for solving the transient heat transfer problems in MATLAB is developed from substituting the constants m, d, c, a, and f as given in Eqs. (8)–(12) with u variable as the temperature (T).

$$m = 0 \tag{8}$$

$$d = \rho C_p t_z \tag{9}$$

$$c = kt_z \tag{10}$$

$$a = 2h_c T + 2\varepsilon\sigma T^4 \tag{11}$$

$$f = 2h_c T_a + 2\varepsilon\sigma T_a^4 \tag{12}$$

The wall panel thickness was considered for the FE model. Geometry was created by dividing the wall thickness into small elements, and as per the previous time step temperature results, each element material properties were defined. Mesh size was selected by considering the convergence of the results. Fire loading was applied to the wall as a temperature boundary condition. The temperature boundary condition was defined as a time-temperature variation as per the standard fire condition. Fig. 11 shows the FE model meshing and results of the FE model and Fig. 12 shows the temperature variation along the wall.

4. Validation of finite element model

Validation of the developed simulation is essential to evaluate the accuracy of the developed models; the assumed simplifications

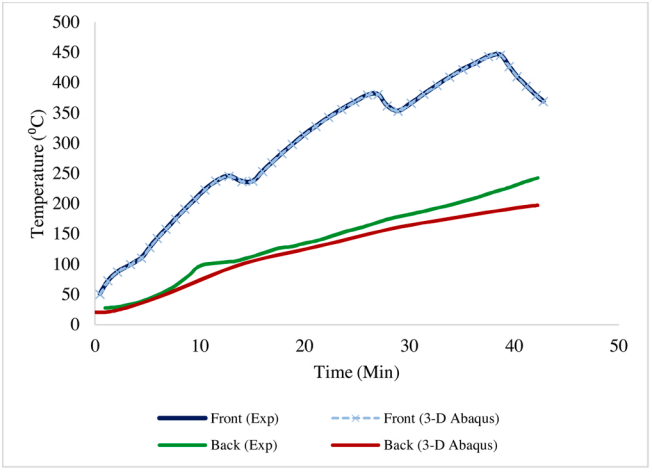

(a)

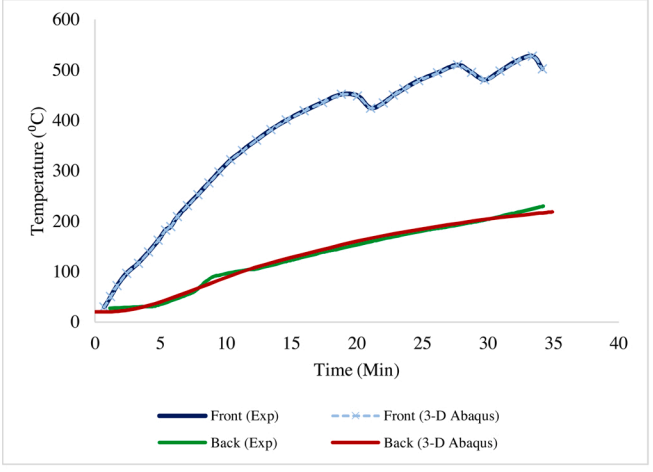

(b)

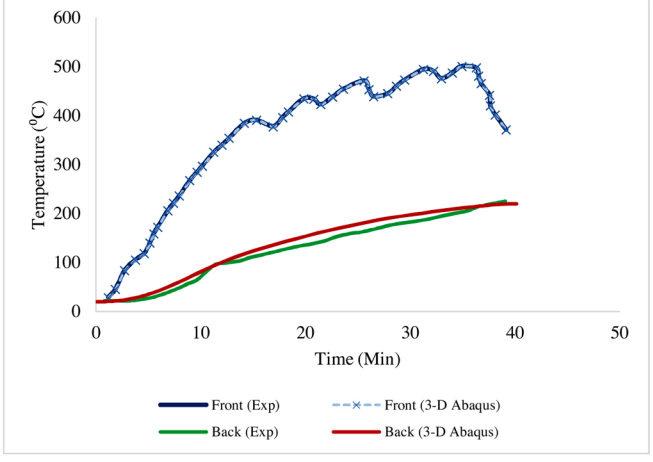

(c)

(caption on next page)

Fig. 14. (a): Comparison of Experimental results with 3-D FEA in ABAQUS results for C3DPC(S1). (b): Comparison of Experimental results with 3-D FEA in ABAQUS results for C3DPC(S2). (c): Comparison of Experimental results with 3-D FEA in ABAQUS results for C3DPC(S3).

Table 1
2-D FEA Validation for 3DPC Samples.

Comparison of Experimental results with 2-D FEA in ABAQUS	Comparison of Experimental results with 2-D FEA in MATLAB
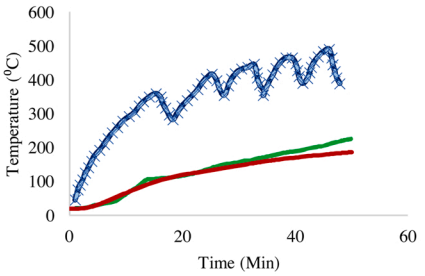 3DPC(S1)	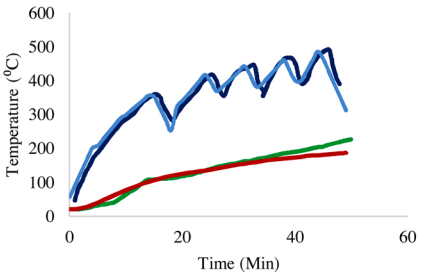 3DPC(S1)
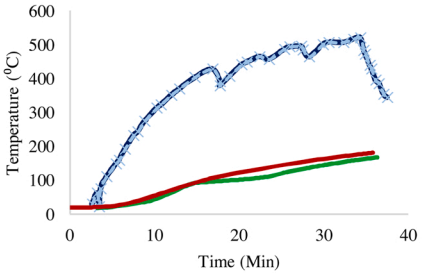 3DPC(S2)	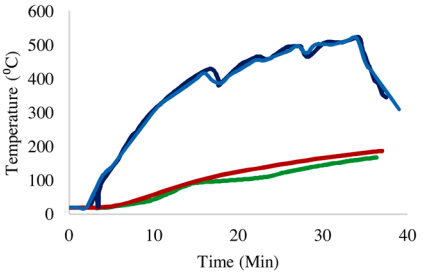 3DPC(S2)
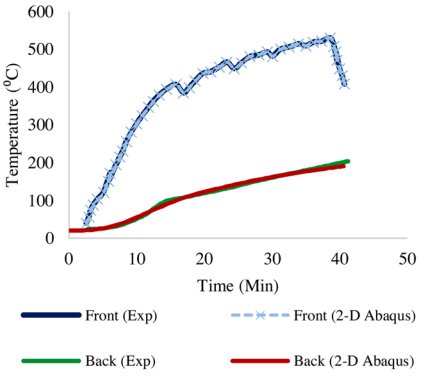 3DPC(S3)	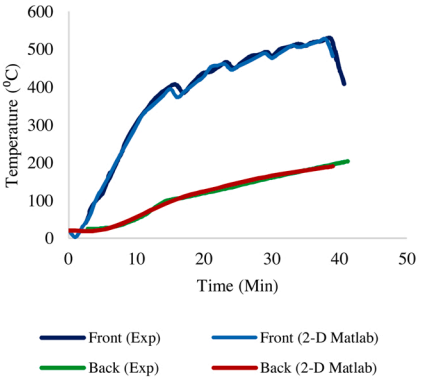 3DPC(S3)

Table 2
2-D FEA Validation for C3CPD Samples.

Comparison of Experimental results with 2-D FEA in ABAQUS	Comparison of Experimental results with 2-D FEA in MATLAB
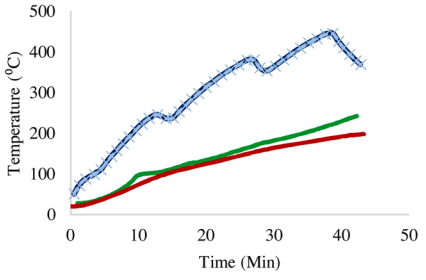 C3DPC(S1)	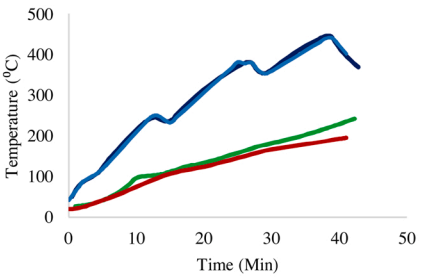 C3DPC(S1)
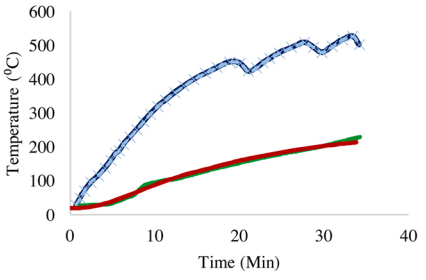 C3DPC(S2)	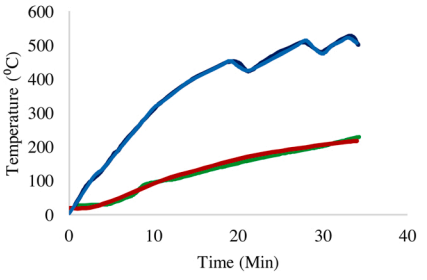 C3DPC(S2)
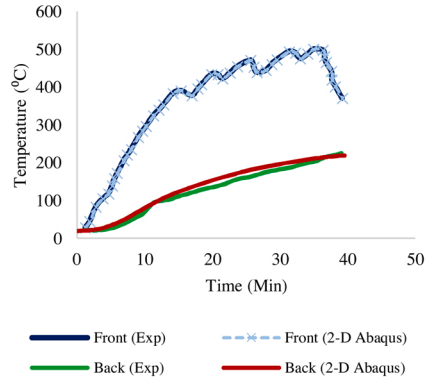 C3DPC(S3)	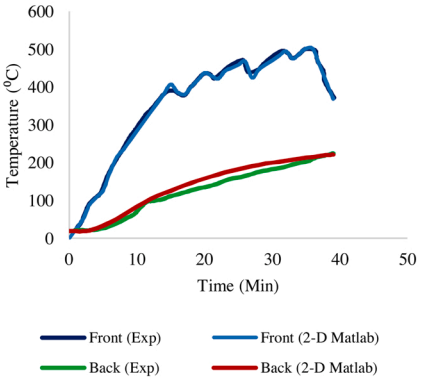 C3DPC(S3)

Table 3
Dimensions of the wall specimens considered in the Investigation (units in mm).

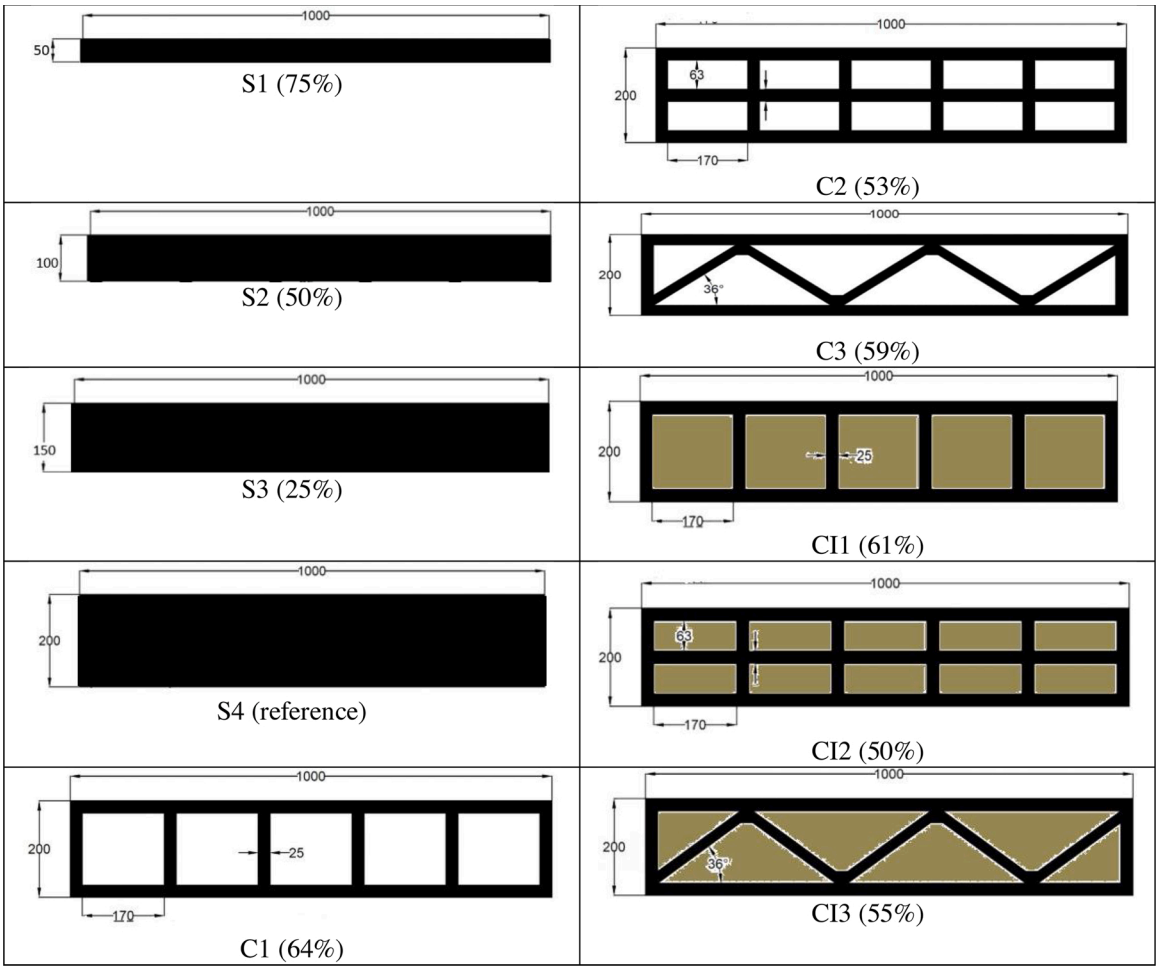

Notes:
S1, S2, S3 & S4 – Solid wall panels of 50 mm, 100 mm, 150 mm and 200 mm thickness.
C1, C2 & C3 – Cavity wall panels.
CI1, CI2 & CI3 – Cavity insulated wall panels.
All dimensions are shown in millimeters.
The percentages within brackets are referred to the weight reduction per unit length of the wall with respect to the S4 specimen.
Weight reduction percentages of Cavity Insulated panels were derived considering the density of Rockwool and concrete as 100 and 2000 kg/m^3.

for the model applications, and the material characterization. Hence, the unexposed surface temperature results obtained from the Finite Element Analysis (FEA) were compared with the experimental results presented by Cicione et al. [32].

Initially, the elevated temperature properties of normal weight concrete available in Eurocode 2 were used as the material model and the midpoint temperature and unexposed surface temperature with time were obtained as results. According to the results, for NCC, the midpoint temperature variation was matching with FE results but slight variation in unexposed temperature variation was identified. For 3DPC and C3DPC models, the unexposed surface temperature and the mid-temperature have shown considerable variations for some samples. The mid-point temperature variations were observed due to the differences in thermocouple placements in the experimental program. Hence, it has been decided to slightly modify the specific heat variation of 3D printed concrete slightly between 20–120 °C temperatures to match the unexposed surface temperature to obtain more accurate results in FE model in 3D

Table 4
Parametric Study Outline.

Density (kg/m^3)	Wall Configuration	Thickness (mm)	Number of models
1800	Solid	50, 100, 150, 200	4
	C1, C2, C3	200	3
	CI1, CI2, CI3	200	3
Sub Total			10
2000	Solid	50, 100, 150, 200	4
	C1, C2, C3	200	3
	CI1, CI2, CI3	200	3
Sub Total			10
2150	Solid	50, 100, 150, 200	4
	C1, C2, C3	200	3
	CI1, CI2, CI3	200	3
Sub Total			10
2250	Solid	50, 100, 150, 200	4
	C1, C2, C3	200	3
	CI1, CI2, CI3	200	3
Sub Total			10
2400	Solid	50, 100, 150, 200	4
	C1, C2, C3	200	3
	CI1, CI2, CI3	200	3
Sub Total			10
Total			50

Table 5
Insulation Fire Rating of Solid Wall Panels.

Wall Specimen (thickness)		S1 (50 mm)	S2 (100 mm)	S3 (150 mm)	S4 (200 mm)
Material Reduction		75 %	50 %	25 %	reference
Insulation Fire Rating (Min) w.r.t. densities	1800 kg/m^3	14	65.5	195	>300
	2000 kg/m^3	15	70	218	>300
	2150 kg/m^3	16	75	232	>300
	2250 kg/m^3	16.5	78	240	>300
	2400 kg/m^3	18	84	255	>300

printed concrete. To achieve this, three different specific heat variations were considered and the variations which give accurate results in predicting the unexposed surface temperature variation was selected. The selected specific heat variation is shown in Fig. 4(c).

Subsequently, experimental results were compared with both ABAQUS and MATLAB models. The comparison of experimental results 3-D FEA in ABAQUS results of the unexposed surface temperature with time of three samples of 3DPC are shown in Fig. 13(a)–(c). Similarly, the time-temperature variations of three C3DPC samples are presented in Fig. 14(a)–(c).

The comparison of experimental results with 2-D FEA in ABAQUS and 2-D FEA in MATLAB is presented in Tables 1 and 2 for 3DPC samples and C3DPC samples respectively.

Experimental curves of unexposed surface temperature show excellent agreement with FEA curves. Since the experimental temperature and FE model temperature results are matching, it could be concluded that modified properties proposed for the 3D printed concrete could be utilized for parametric analysis of insulation fire performance of 3D printed concrete walls.

5. Insulation fire ratings of 3D printed concrete wall panels with different parameters

5.1. General

As per the previous section 2D and 3D models have been developed and validated against available experimental results, 3D Heat transfer FE analysis for different wall configurations was performed using ABAQUS CAE the commercially available software. Then the

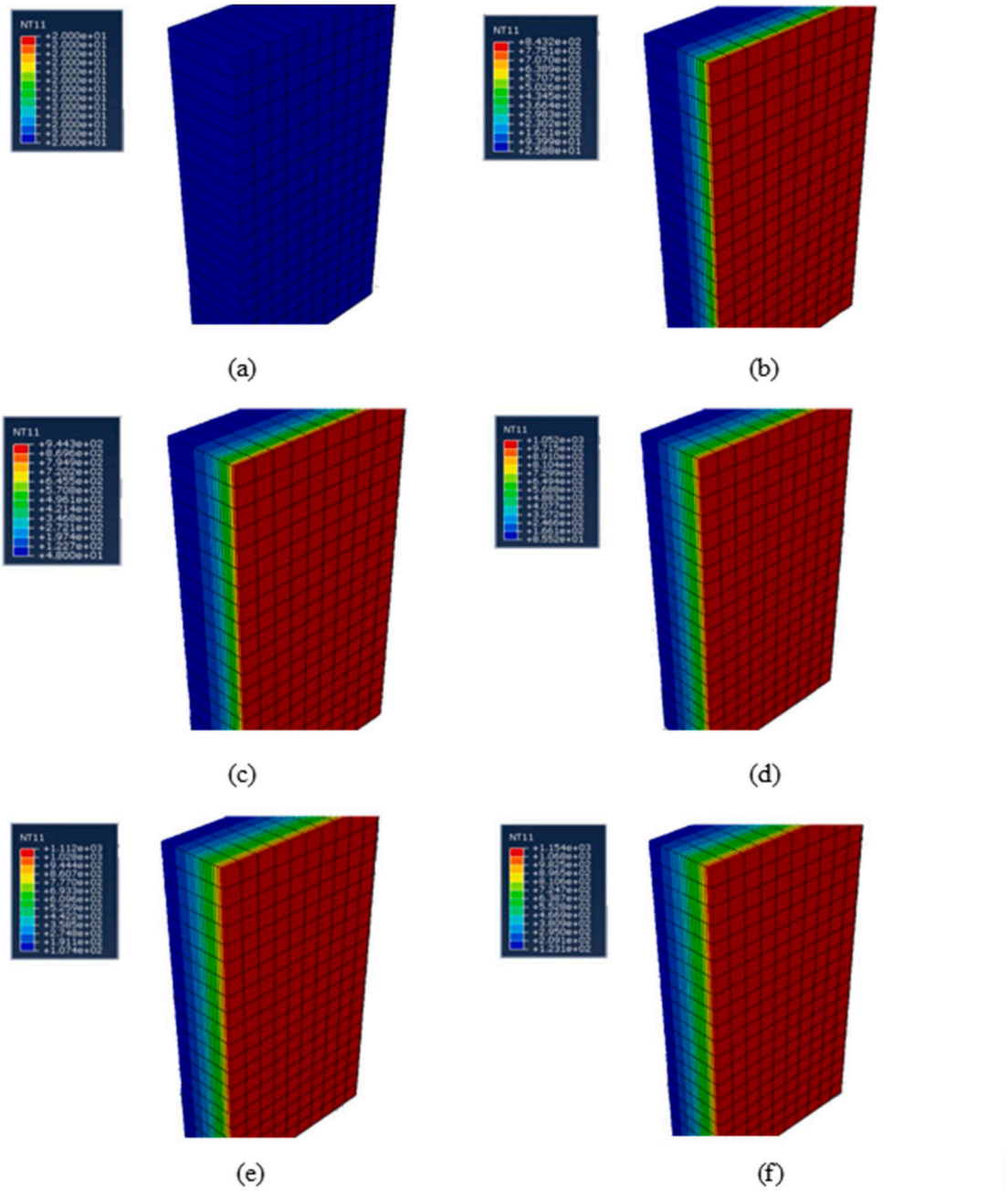

Fig. 15. Temperature contours of 200 mm solid wall at different time intervals; (a) 0 min, (b) 30 min, (c) 1 h, (d) 2 h, (e) 3 h, (f).4 h.

Table 6
Insulation Fire Rating of Cavity Wall Panels.

Wall Specimen (thickness)		C1 (200 mm)	C2 (200 mm)	C3 (200 mm)	S4 (200 mm)
Material Reduction		64 %	53 %	59 %	reference
Insulation Fire Rating (min) w.r.t. densities	1800 kg/m^3	44	110	72	>300
	2000 kg/m^3	48	120	78	>300
	2150 kg/m^3	50	130	83	>300
	2250 kg/m^3	52	132	87	>300
	2400 kg/m^3	55	138	91	>300

Table 7
Comparison of Insulation Fire Rating.

Wall configurations	Excess material requirement (volume %)	Insulation Fire Rating Enhancement (%)				
		1800 kg/m^3	2000 kg/m^3	2150 kg/m^3	2250 kg/m^3	2400 kg/m^3
C2 compared to C1	17	60	60	61.5	60.5	60
C2 compared to C3	10	34.5	35	36	34	31
C3 compared to C1	8	39	38	40	40	39

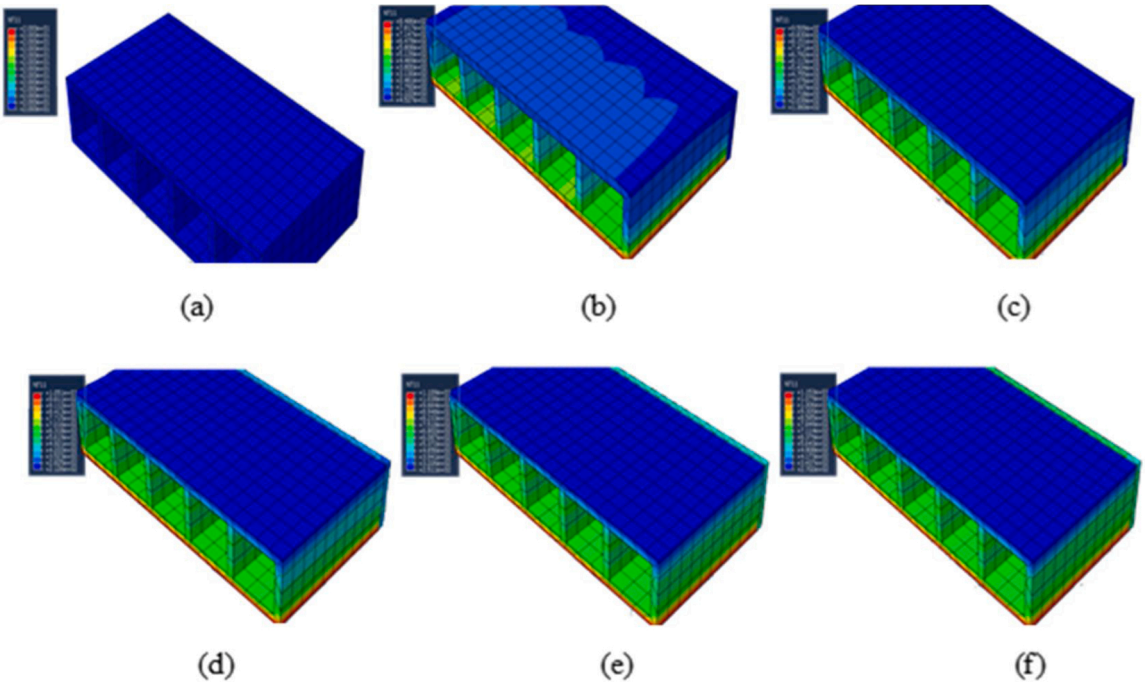

Fig. 16. Temperature contours of C1 wall panel at different time intervals; (a) 0 min, (b) 30 min, (c) 1 h, (d) 2 h, (e) 3 h, (f).4 h.

developed FE model was used to determine the insulation fire ratings of non-load bearing wall panels. Hence, the model was extended to study ten 3D printed wall specimens against several parameters such as density of the concrete material, wall thickness and different wall configurations with and without cavity insulation.

5.2. Wall panel specimens

3D printed solid wall panels with different thicknesses are used in the industry for better thermal and acoustic characteristics. When the thickness of the wall is increased, energy and acoustic performance being enhanced however, compensating on material costs and carbon foot print. The most critical issue with thick concrete wall panels is the challenging nature of handling the panels at the construction site, due to increased weight. Complying with currently available 3D printed wall panels in the industry, wall thicknesses of 50, 100, 150 and 200 mm have been chosen to observe the effect of thickness of the wall panels for the fire performance.

Moreover, three innovative cavity wall panel specimens of 200 mm overall thickness have been selected in order to reduce the overall panel weight. Those three wall panels integrating the Rockwool cavity insulation were also studied as three additional wall specimens. Table 3 presents the cross-sections and dimensions of wall specimens that have been investigated in the study.

3DPC elements applied in the construction industry exhibit densities ranging from 1800 to 2400 kg/m^3 [8,11–14]. At the same time density of the material has a great influence on the heat transfer model which determines the time-dependent temperature through

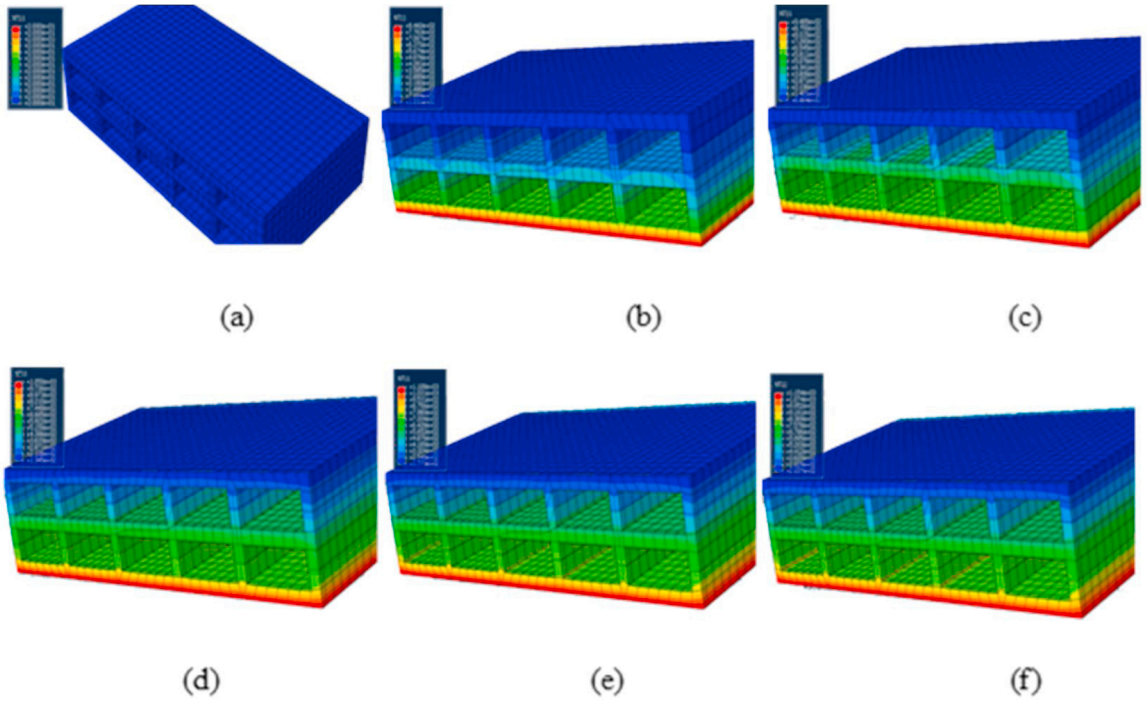

Fig. 17. Temperature contours of C2 wall at different time intervals; (a) 0 min, (b) 30 min, (c) 1 h, (d) 2 h, (e) 3 h, (f).4 h.

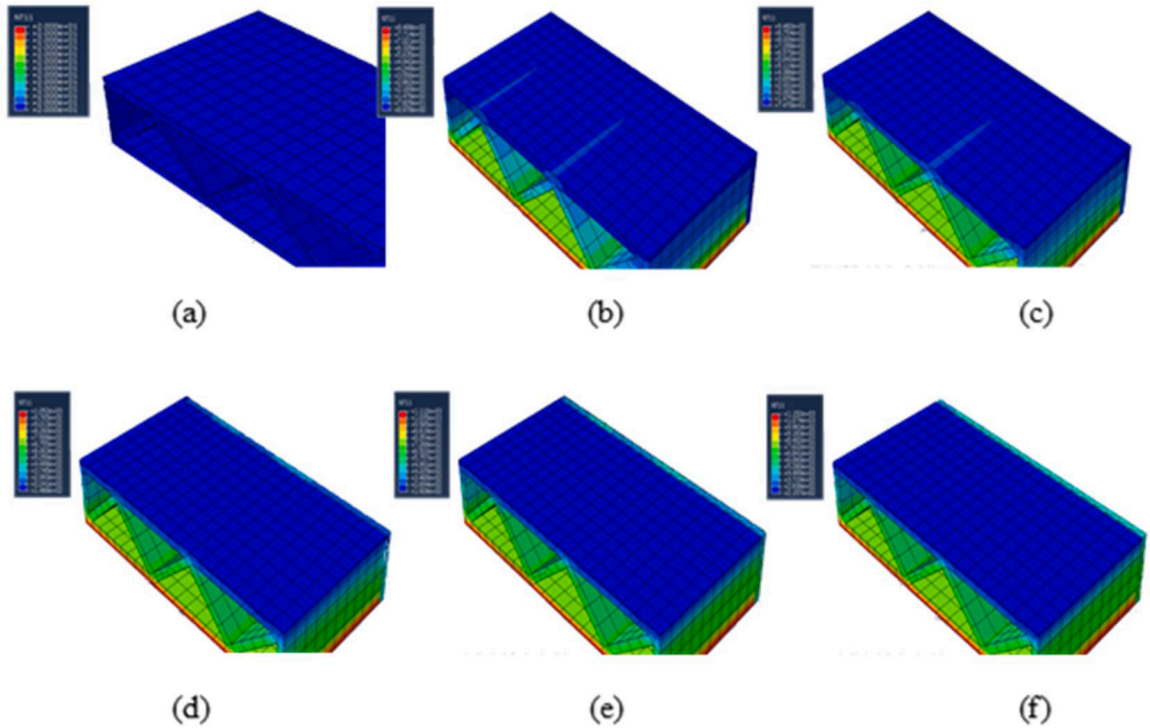

Fig. 18. Temperature contours of C3 wall at different time intervals; (a) 0 min, (b) 30 min, (c) 1 h, (d) 2 h, (e) 3 h, (f).4 h.

Table 8
Insulation Fire Rating of Rockwool Insulated Wall Specimens.

Wall Specimen (thickness)		CI1 (200 mm)	CI2 (200 mm)	CI3 (200 mm)	S4 (200 mm)
Material Reduction		61%	50%	55%	reference
Insulation Fire Rating (min) w.r.t. densities	1800 kg/m^3	>300			
	2000 kg/m^3				
	2150 kg/m^3				
	2250 kg/m^3				
	2400 kg/m^3				

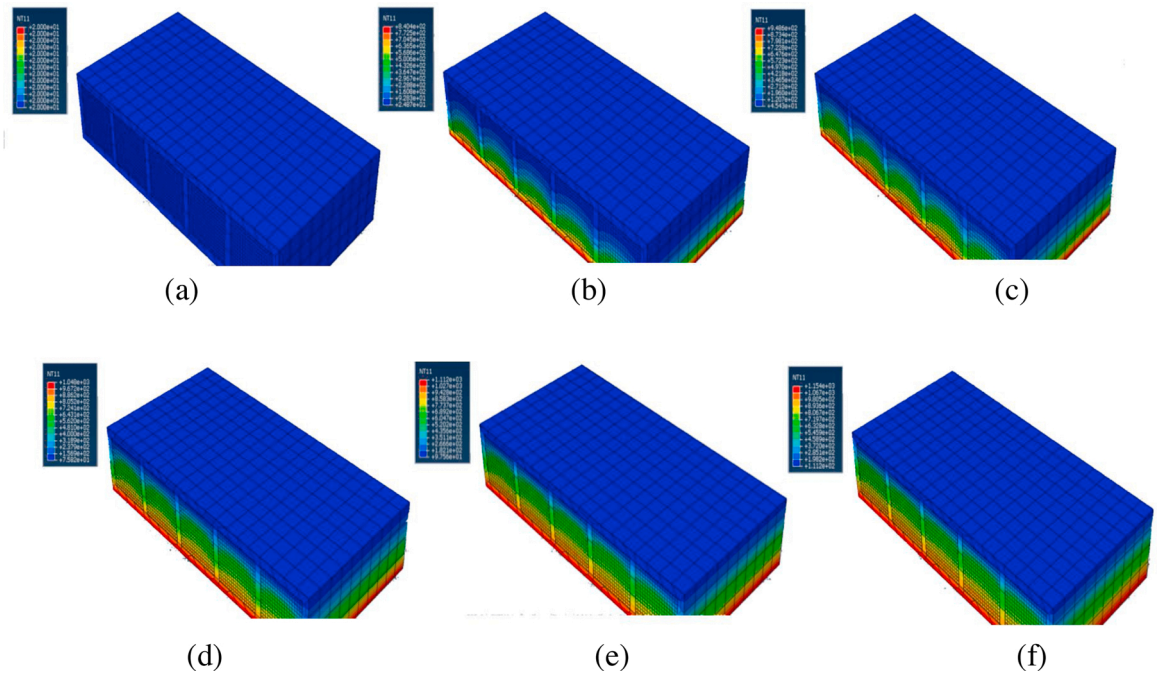

Fig. 19. Temperature contours of CI1 wall at different time intervals; (a) 0 min, (b) 30 min, (c) 1 h, (d) 2 h, (e) 3 h, (f).4 h.

wall specimens in case of a fire accident [15,16]. Hence, the density of concrete material was identified as a dominant parameter that affects the Fire Resistance Level (FRL) and five density values were selected for the heat transfer analyses of the ten wall configurations. i.e.: 1800, 2000, 2150, 2250 and 2400 kg/m^3. Therefore, the parametric study consists of fifty (50) non load bearing 3D printed wall specimens, which have been numerically analyzed for the FRL based on insulation criterion. The details of parametric study are presented in Table 4.

6. Results and discussion

The standard fire curve, ISO 834 was applied on firesides of the heat transfer Finite Element Models (FEM) of wall specimens and the time-dependent unexposed side temperature was determined from ABAQUS CAE tools. Since the unexposed side temperature rise should not exceed 140°C in average and 200°C at any point to satisfy the fire resistance in insulation criterion according to Eurocode 2 [35], the insulation fire rating values were determined from the unexposed side temperature variation of each wall specimen.

6.1. Solid wall panels

The FRL based on insulation criterion of S1, S2, S3 and S4 solid wall specimens with respect to the density of concrete and thickness

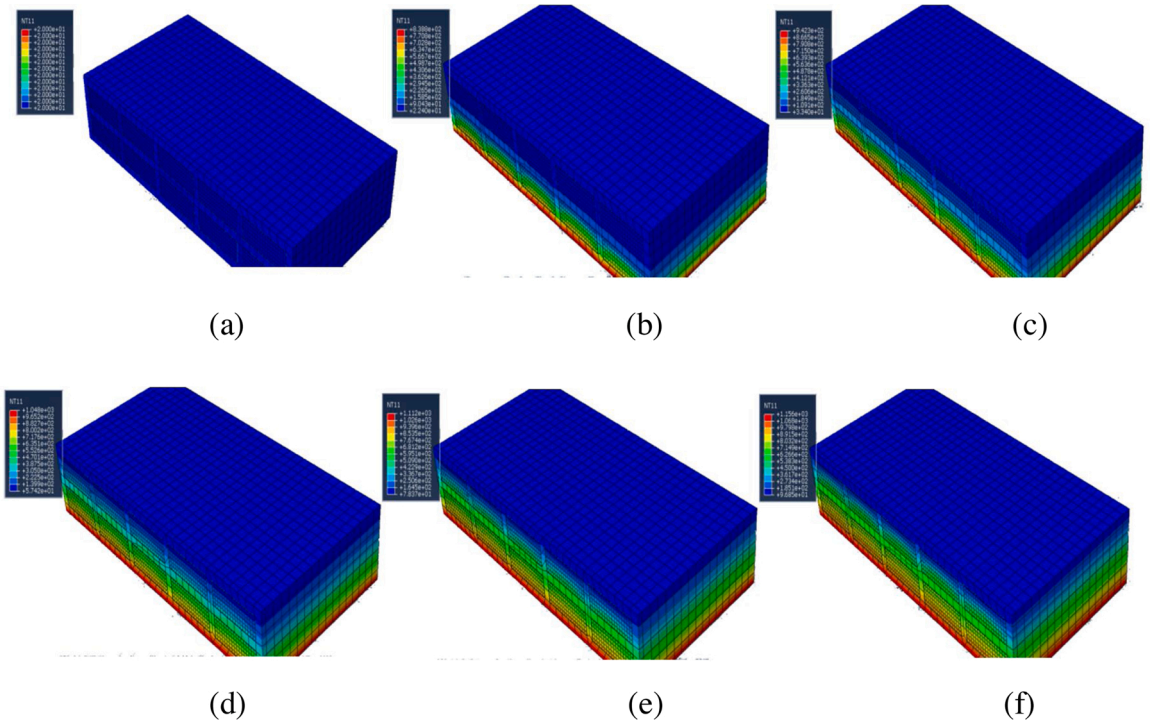

Fig. 20. Temperature contours of CI2 wall at different time intervals; (a) 0 min, (b) 30 min, (c) 1 h, (d) 2 h, (e) 3 h, (f).4 h.

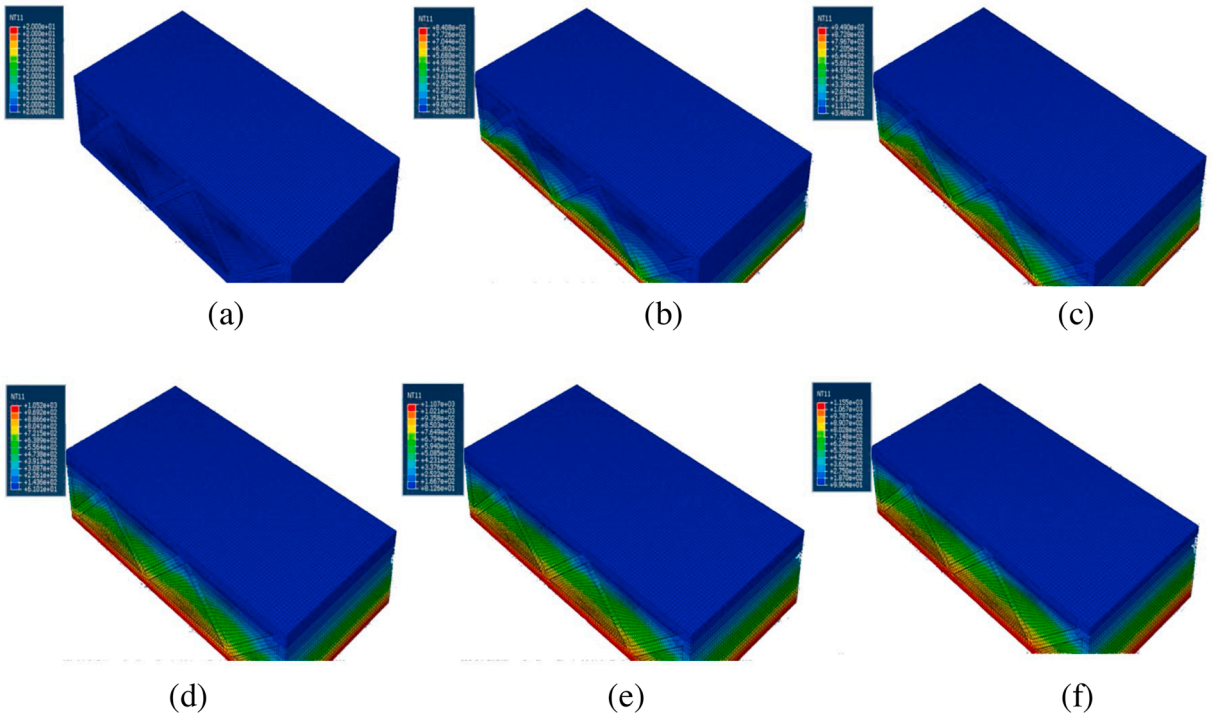

Fig. 21. Temperature contours of CI3 wall at different time intervals; (a) 0 min, (b) 30 min, (c) 1 h, (d) 2 h, (e) 3 h, (f).4 h.

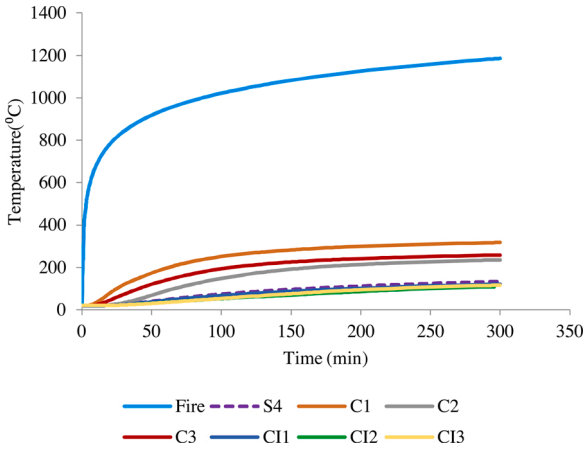

Fig. 22. Comparison of Unexposed Surface temperature variation of all the wall configurations with 1800 kg/m^3 with standard fire.

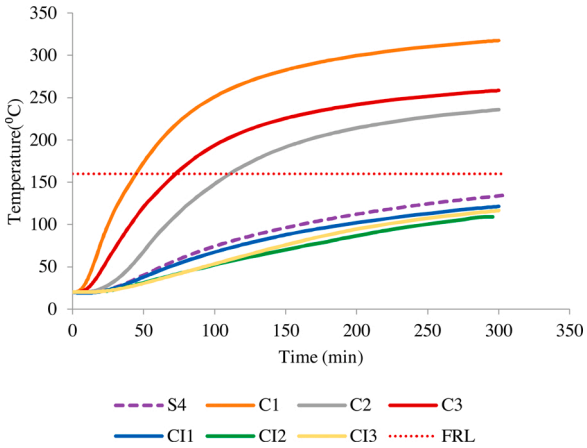

Fig. 23. Comparison of Unexposed Surface temperature variation of all the wall configurations with 1800 kg/m^3 under standard fire condition.

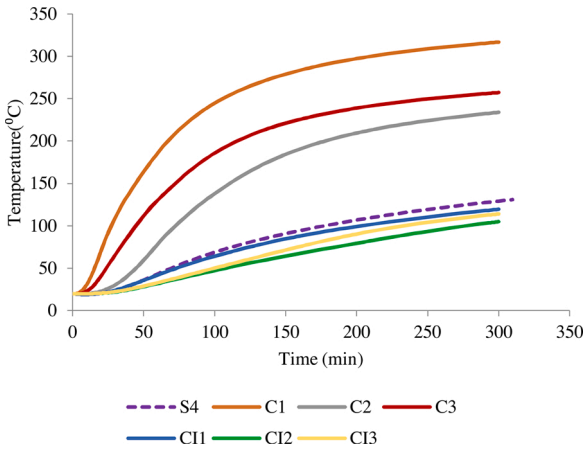

Fig. 24. Comparison of Unexposed Surface temperature variation of all the wall configurations with 2000 kg/m^3 under standard fire condition.

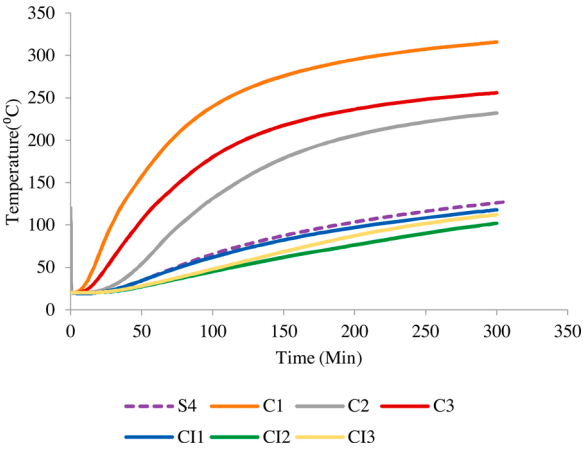

Fig. 25. Comparison of Unexposed Surface temperature variation of all the wall configurations with 2150 kg/m^3 under standard fire condition.

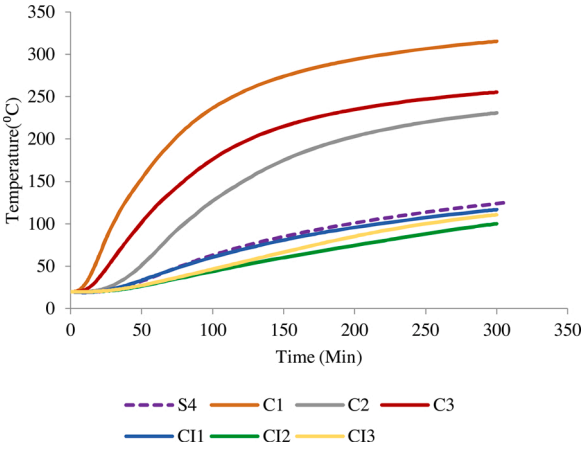

Fig. 26. Comparison of Unexposed Surface temperature variation of all wall configurations with 2250 kg/m^3 under standard fire condition.

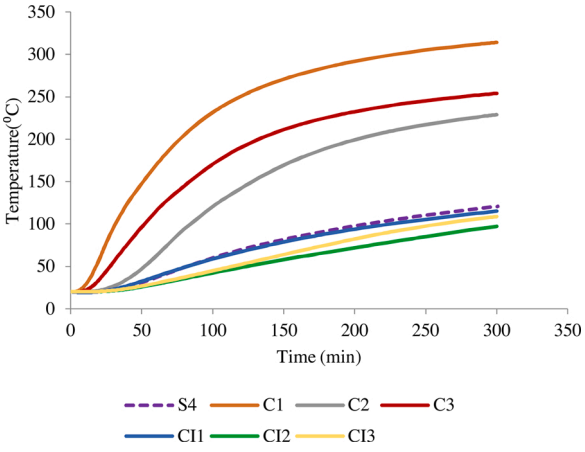

Fig. 27. Comparison of Unexposed Surface temperature variation of all wall configurations with 2400 kg/m^3 under standard fire condition.

of the wall has been summarised in Table 5. The results show the variation of insulation fire rating of the solid walls with different wall thickness and different material densities. It is clearly seen that the insulation fire rating is increasing with the increase in density for all the wall panels regardless the thickness. Moreover, the insulation fire rating increment is visible with increasing wall thickness.

Fig. 15 demonstrates the temperature distribution of the solid wall S4 (200 mm) model at 0 min, 30 min, 1 h, 2 h, 3 h and 4 h of exposure to the standard fire ISO 834.

6.2. Cavity wall panels

The insulation criterion based FRL of C1, C2 and C3 cavity wall specimens has been compared against the reference S4 solid wall specimen as presented in Table 6. Solid wall configuration showed better fire performance compared to the cavity wall configurations. Considerable reduction in insulation fire rating has been identified for all three different configurations. However, Cavity wall configuration 2 showed the improved fire performance compared to the other two configurations. The comparison of insulation fire rating among the considered three cavity wall configurations is presented in Table 7.

According to the results displayed in Table 7, cavity wall configuration 2 (C2) exhibits 60 % enhanced fire performance in average with 17 % additional material compared to cavity wall configuration 1 (C1). Similarly it shows an increased fire performance of 34 % in average with 10 % additional material requirement compared to cavity wall configuration 3 (C3). Moreover, C3 behaves better than C1 for fire.

Figs. 16–18 illustrate the temperature distribution of the cavity wall panel models C1, C2 and C3 at 0 min, 30 min, 1 h, 2 h, 3 h and 4 h of exposure to the standard fire.

6.3. Rockwool insulated composite wall panels

In order to improve the behaviour of the same three cavity wall configurations towards fire exposure Rockwool has been used as a cavity filling material. The unexposed surface temperature under standard fire condition was considered and the insulation fire rating for each configuration was determined. Insulation based fire rating of the Rockwool insulated cavity wall specimens are compared against the reference S4 solid wall panel is shown in Table 8.

Introducing Rockwool as a filling material has increased the fire performance considerably. The insulation fire rating higher than 5 h (300 min) has been achieved with 61 %, 50 % and 55 % of material reduction for CI1, CI2 and CI3 respectively compared to the solid wall panel. Figs. 19–21 illustrate the temperature distribution of the cavity insulated wall panel models CI1, CI2 and CI3 at 0 min, 30 min, 1 h, 2 h, 3 h and 4 h of exposure to the standard fire. Fig. 22 shows the time temperature variation of the wall configuration with 1800 kg/m^3 with standard fire exposure. Figs. 23–27 illustrate the comparison of unexposed surface temperature variation of all the wall configurations under standard fire condition for considered material densities.

7. Conclusions

This paper has presented the results of numerical analyses on the thermal performance of 3DPC walls that included both the conventional cavity walls and the new composite wall configurations. It involved details of FEM of 3DPC walls, thermal results from heat transfer analysis under standard fire conditions, and their validation with fire test results. The developed FEM showed a good agreement with transient time-temperature profiles obtained from experiments. In total 50 FEMs of 3DPC walls with three different configurations (solid, cavity, and composite) and with different densities were developed to simulate the thermal behaviour. The proposed thermal properties for 3DPC concrete, which were successfully validated against fire test results, were employed in FEMs. Numerical analysis showed that non-load bearing 3DPC cavity walls were detrimental to the insulation failure fire rating while 3DPC solid walls resulted in a superior fire rating. The considered cavity walls were up to 64 % lesser in weight compared to solid walls. While maintaining substantial weight reduction and to improve the insulation fire rating of 3DPC cavity walls, a novel composite system of Rockwool cavity insulation was examined. The novel composite 3DPC wall configuration demonstrated significant enhancement of insulation fire rating with negligible increment of the total weight. Therefore, novel composite non-load bearing 3DPC wall configurations are proposed to be employed in construction to achieve superior insulation fire rating with substantial material saving compared to solid 3DPC walls.

8. Future recommendation

In this study, the temperature dependent thermal properties of normal concrete were employed with suitable modifications in the development of FE models for 3D printed concrete. No work had been carried out on the variation of thermal properties with temperature such as thermal conductivity, specific heat capacity and density of 3D printable concrete mixture. Hence, thermal properties of 3D printable concrete at elevated temperatures should be determined and studied in the near future. Moreover, the fire behaviour of 3D printed concrete walls made with different void sections is yet to be assessed.

Declaration of Competing Interest

The authors declare that they have no known competing financial interests or personal relationships that could have appeared to influence the work reported in this paper.

Acknowledgements

The Authors would like to acknowledge the financial and technical support of Northumbria University and University of Sri Jayewardenepura.

References

[1] R.A. Buswell, W.R. Leal de Silva, S.Z. Jones, J. Dirrenberger, 3D printing using concrete extrusion: a roadmap for research, Cem. Concr. Res. 112 (2018) 37–49.
[2] G. De Schutter, K. Lesage, V. Mechtcherine, V.N. Nerella, G. Habert, I. Agusti-Juan, Vision of 3D printing with concrete — Technical, economic and environmental potentials, Cem. Concr. Res. 112 (2018) 25–36.
[3] F. Beyhan, S. Arslan Selçuk, 3D printing in architecture: one step closer to a sustainable built environment, Proceedings of 3rd International Sustainable Buildings Symposium (ISBS 2017) (Lecture Notes in Civil Engineering (2018) 253–268.
[4] B. Nematollahi, M. Xia, J. Sanjayan, Current progress of 3D concrete printing technologies, Presented at the Proceedings of the 34th International Symposium on Automation and Robotics in Construction (ISARC) (2017).
[5] P. Wu, J. Wang, X. Wang, A critical review of the use of 3-D printing in the construction industry, Autom. Constr. 68 (2016) 21–31.
[6] C. Balletti, M. Ballarin, F. Guerra, 3D printing: state of the art and future perspectives, J. Cult. Herit. 26 (2017) 172–182.
[7] B. Panda, S.C. Paul, L.J. Hui, Y.W.D. Tay, M.J. Tan, Additive manufacturing of geopolymer for sustainable built environment, J. Clean. Prod. 167 (2017) 281–288.
[8] A.S.J. Suiker, Mechanical performance of wall structures in 3D printing processes: theory, design tools and experiments, Int. J. Mech. Sci. 137 (2018) 145–170.
[9] P. Feng, X. Meng, J.-F. Chen, L. Ye, Mechanical properties of structures 3D printed with cementitious powders, Constr. Build. Mater. 93 (2015) 486–497.
[10] T.T. Le, S.A. Austin, S. Lim, R.A. Buswell, A.G.F. Gibb, T. Thorpe, Mix design and fresh properties for high-performance printing concrete, Mater. Struct. 45 (8) (2012) 1221–1232.
[11] T.T. Le, et al., Hardened properties of high-performance printing concrete, Cem. Concr. Res. 42 (3) (2012) 558–566.
[12] B. Panda, S. Chandra Paul, M. Jen Tan, Anisotropic mechanical performance of 3D printed fiber reinforced sustainable construction material, Mater. Lett. 209 (2017) 146–149.
[13] R.J.M. Wolfs, F.P. Bos, T.A.M. Salet, Early age mechanical behaviour of 3D printed concrete: numerical modelling and experimental testing, Cem. Concr. Res. 106 (2018) 103–116.
[14] *Apis Cor Built The Office With A Robotic Printer*. [image] Available at: <https://www.dezeen.com/2019/12/22/apis-cor-worlds-largest-3d-printed-building-dubai/> (Accessed 10 June 2020).
[15] J.J. del Coz-Díaz, J.E. Martínez-Martínez, M. Alonso-Martínez, F.P. Álvarez Rabanal, Comparative study of LightWeight and Normal Concrete composite slabs behaviour under fire conditions, Eng. Struct. 207 (2020).
[16] S. Banerji, V. Kodur, R. Solhmirzaei, Experimental behavior of ultra high performance fiber reinforced concrete beams under fire conditions, Eng. Struct. 208 (2020).
[17] V.D. Cao, T.Q. Bui, A.-L. Kjøniksen, Thermal analysis of multi-layer walls containing geopolymer concrete and phase change materials for building applications, Energy 186 (2019).
[18] L.-H. Han, K. Zhou, Q.-H. Tan, T.-Y. Song, Performance of steel reinforced concrete columns after exposure to fire: numerical analysis and application, Eng. Struct. 211 (2020).
[19] X. Liang, C. Wu, Y. Yang, Z. Li, Experimental study on ultra-high performance concrete with high fire resistance under simultaneous effect of elevated temperature and impact loading, Cem. Concr. Compos. 98 (2019) 29–38.
[20] E. Ryu, H. Kim, Y. Chun, I. Yeo, Y. Shin, Effect of heated areas on thermal response and structural behavior of reinforced concrete walls exposed to fire, Eng. Struct. 207 (2020).
[21] P. Weerasinghe, K. Nguyen, P. Mendis, M. Guerrieri, Large-scale experiment on the behaviour of concrete flat slabs subjected to standard fire, J. Build. Eng. 30 (2020).
[22] Y. Zhang, Y. Zhang, G. Liu, Y. Yang, M. Wu, B. Pang, Fresh properties of a novel 3D printing concrete ink, Constr. Build. Mater. 174 (2018) 263–271.
[23] B. Panda, M.J. Tan, Rheological behavior of high volume fly ash mixtures containing micro silica for digital construction application, Mater. Lett. 237 (2019) 348–351.
[24] B. Nematollahi, P. Vijay, J. Sanjayan, A. Nazari, M. Xia, V.N. Nerella, V. Mechtcherine, Effect of polypropylene fibre addition on properties of geopolymers made by 3D printing for digital construction, Materials (Basel) 11 (12) (2018). Nov 22.
[25] S.C. Paul, Y.W.D. Tay, B. Panda, M.J. Tan, Fresh and hardened properties of 3D printable cementitious materials for building and construction, Arch. Civ. Mech. Eng. 18 (1) (2018) 311–319.
[26] A. Kazemian, X. Yuan, E. Cochran, B. Khoshnevis, Cementitious materials for construction-scale 3D printing: laboratory testing of fresh printing mixture, Constr. Build. Mater. 145 (2017) 639–647.
[27] V.N. Nerella, M. Näther, A. Iqbal, M. Butler, V. Mechtcherine, Inline quantification of extrudability of cementitious materials for digital construction, Cem. Concr. Compos. 95 (2019) 260–270.
[28] B. Zareiyan, B. Khoshnevis, Effects of interlocking on interlayer adhesion and strength of structures in 3D printing of concrete, Autom. Constr. 83 (2017) 212–221.
[29] J.G. Sanjayan, B. Nematollahi, M. Xia, T. Marchment, Effect of surface moisture on inter-layer strength of 3D printed concrete, Constr. Build. Mater. 172 (2018) 468–475.
[30] L. Wang, H. Jiang, Z. Li, G. Ma, Mechanical behaviors of 3D printed lightweight concrete structure with hollow section, Arch. Civ. Mech. Eng. 20 (1) (2020).
[31] Y. Weng, et al., Printability and fire performance of a developed 3D printable fibre reinforced cementitious composites under elevated temperatures, Virtual Phys. Prototyp. 12/11 (2018).
[32] A. Cicione, J. Kruger, R.S. Walls, G. Van Zijl, An experimental study of the behavior of 3D printed concrete at elevated temperatures, Fire Saf. J. (2020).
[33] S. Ni, T. Gernay, Considerations on computational modeling of concrete structures in fire, Fire Saf. J. (2020).
[34] ABAQUS, Hibbitt, Karlsson & Sorensen, Inc. Pawtucket, USA.
[35] EN 1992-1-2, Eurocode 2: Design of Concrete Structures - Part 1-2: General Rules - Structural Fire Design, 2017.
[36] M. Rusthi, P. Keerthan, M. Mahendran, A. Ariyanayagam, Investigating the fire performance of LSF wall systems using finite element analyses, J. Struct. Fire Eng. 8 (4) (2017) 354–376.
[37] P. Keerthan, M. Mahendran, Thermal performance of composite panels under fire conditions using numerical studies: plasterboards, Rockwool, glass fibre and cellulose insulations, Fire Technol. 49 (2) (2012) 329–356.
[38] E. Steau, P. Keerthan, M. Mahendran, 10.15: thermal modelling of LSF floor systems made of lipped channel and hollow flange channel section joists, ce/papers 1 (2–3) (2017) 2638–2647.
[39] Y. Dias, P. Keerthan, M. Mahendran, Predicting the fire performance of LSF walls made of web stiffened channel sections, Eng. Struct. 168 (2018) 320–332.